Journal of Materials Chemistry A

Highly Efficient Organic Solar Cells with Superior Deformability Enabled by Diluting Small Molecule Acceptor Content

Journal:	*Journal of Materials Chemistry A*
Manuscript ID	TA-ART-02-2022-000959.R1
Article Type:	Paper
Date Submitted by the Author:	22-Feb-2022
Complete List of Authors:	Zhu, Qinglian; Xi'an Jiaotong University, State Key Laboratory for Mechanical Behavior of Materials xue, jingwei; Xi'an Jiaotong University Zhao, Heng; Xi'an Jiaotong University, State Key Laboratory for Mechanical Behavior of Materials Lin, Baojun; State Key Laboratory for Mechanical Behavior of Materials, Xi'an Jiaotong University, Xi'an 710049, China Bi, Zhaozhao; Xi'an Jiaotong University, b. State Key Laboratory for Mechanical Behavior of Materials Seibt, Susanne; Australian Synchrotron Zhou, Ke; Xi'an Jiaotong University, Mechanical Behavior of Materials Ma, Wei; Xi'an Jiaotong University, State Key Laboratory for Mechanical Behavior of Materials

Highly Efficient Organic Solar Cells with Superior Deformability Enabled by Diluting Small Molecule Acceptor Content

Qinglian Zhu[a], Jingwei Xue[a], Heng Zhao[a], Baojun Lin[a], Zhaozhao Bi[a], Susanne Seibt[b], Ke Zhou[a], Wei Ma[a,*]

[a]State Key Laboratory for Mechanical Behavior of Materials Xi'an Jiaotong University, Xi'an 710049, China

[b]Australian Synchrotron, ANSTO, Clayton, Victoria 3168, Australia.

*Corresponding author. E-mail: msewma@xjtu.edu.cn (W. M.)

Abstract

Developing efficient organic solar cells (OSCs) with strong mechanical deformability is urgent to be addressed to promise their operational reliability in wearable electronics. However, it is challenging to achieve mechanical robust polymer/small molecule OSCs with efficiency over 17% due to abundant brittle donor/acceptor (D/A) interface. Deceasing small molecule content can reduce brittle D/A interface area to enhance deformability, but it may also cause discontinuous electron-conducting regions and thus deteriorates photovoltaic performance. Here, we incorporate polymer donor (D18) into binary PTQ10: m-BTP-PhC6 system under constant PTQ10: m-BTP-PhC6 ratio of 1:1.2 to minimize D/A interfacial area and modulate phase separation, subsequently to fabricate mechanically reliable OSCs with high efficiency. The large incorporation of D18 molecules shows small destruction over m-BTP-PhC6 crystallization because of the poor interaction between D18 and two host materials, affording sufficient pathways for efficient charge percolation under large D/A ratio. More importantly, highly aggregated m-BTP-PhC6 molecules help to minimize D/A interfacial area, enabling ternary films with better deformability than their binary counterparts. As the result, ternary OSCs with large D/A ratio of 1.5:1.2 exhibits high efficiency of 17.3% with crack-onset strain (COS) of 8.8%, which significantly outperforms its binary counterpart with efficiency of 13.8% and COS of 4.4%. Diluting content of small molecules and controlling intermolecular interaction through introducing the second polymer donor represents a promising strategy to fabricate efficient OSCs with superior deformability.

Keywords: ternary organic solar cells, mechanical properties, intermolecular interaction, donor/acceptor ratio tolerance

INTRODUCTION

Organic solar cells (OSCs) with strong mechanical robustness and superior power conversion efficiency (PCE) are highly desirable for the next-generation mobile power supply equipment and diverse Internet of things (IoT) applications.[1-3] Plenty of strategies including molecular structure innovation and morphology optimization have been successfully applied to boost the efficiency of OSCs around 17%-19%.[4-12] However, these strategies typically fail to enhance the mechanical properties of active layers.[13, 14] For instance, increasing the backbone planarity, which is generally regarded as a feasible molecular design rule to improve charge transport ability along conjugated plane to enhance the photon-to-electron conversion efficiency, always deteriorates the mechanical performance since it makes molecules less deformable.[13] Similarly, morphology optimization for efficient OSCs has mainly followed the rule of increasing crystallinity to decrease the charge trap formation, which always embrittles the films by weakening the linkage between different crystallized region.[14, 15] This mutual contradiction between mechanical and photovoltaic property significantly impedes the progress to fabricate high-efficiency while mechanically durable OSCs.

Researchers have made tremendous efforts to improve the mechanical properties without compromising the photovoltaic performances, such as incorporating insulating elastomers and constructing all polymer solar cells with high molecular weight. Ye and coworkers tried to add insulating elastomers SEBS into PM6/N3 system to help dissipate the external stress on semiconducting films.[16] The crack-onset strain (COS) of active layers could be enhanced from 6.9% to 11.2% for those without and with 10% SEBS content incorporation, however, the PCE also dropped from 15.4% to 14.2% at the same time because of the large amount of self-aggregated SEBS region. Kim and coworkers replaced elastomer with fullerene as the third component to overcome the PCE decrease caused by the insulating characteristic of elastomers. As a result, the efficiency enjoyed an enhancement from 5.91% to 6.80% with 30% fullerene addition. Nevertheless, the stretchability of active

layers slightly decreased due to the brittle nature of fullerene.[17] Replacing the brittle small molecules with high molecular weight polymer acceptor to introduce strong intermolecular chain entanglements is another common strategy to construct mechanically robust OSCs. However, the mechanically robust all-polymer photoactive films have only been able to return a device efficiency no more than 11%,[18-22] which are far lower than the reported high-efficiency all polymer OSCs with efficiency around 14%-15%.[23-28] The relatively poor PCE stems from the high molecular weight indispensable to introduce large number of chain entanglements,[29] which could induce poor morphology with large domains reported by Min et.al.[24] Therefore, deformable OSCs with high efficiency, especially those with PCE reaching requirement of practical applications (over 17%), are barely reported[21, 30, 31].

Polymer:small molecule solar cells are the most suitable candidate to be used as the wearable OSCs in the future in terms of their extreme superior efficiency compared with their all polymer or all small molecule counterparts. However, blending polymer donor with small molecule acceptor always results in the significant deterioration of deformability even if the neat polymer donor films are very ductile.[13] The brittleness of small molecules, caused by their strong tendency to form strong crystalline packing and the lack of effective intermolecular entanglements, easily makes the film crack from the small molecule-rich region in the blend.[21, 31-33] It is reasonable to promote the deformability by decreasing the relative content of small molecules to reduce the vulnerable portion of the active layer. Followed by this, Lipomi and coworkers tried to improve the mechanical strength of P3HpT: PCBM by varying the content of PCBM.[13] As the result, COS of blend films were enhanced from 4% to 16% when the relative donor:acceptor (D/A) ratio decreased from 1:0.5 to 1:0.25. However, discontinuous electron-conducting regions induced by insufficient content of PCBM also leaded to the significant loss in photovoltaic performance. Therefore, how to maintain the continuous interpenetrating network under large D/A ratio in high-efficiency OSC needs to be systematic explored.

In this work, PTQ10:m-BTP-PhC6 binary system was selected as the model system to explore the effect of gradually increased D/A ratio on morphology and thus on the

mechanical and photovoltaic performance. Because of the amorphous characteristic of PTQ10, increasing the content of PTQ10 significantly inhibited the crystallization of m-BTP-PhC6 in binary PTQ10:m-BTP-PhC6 films, leading to a significant drop in PCE from 16.9% of 1:1.2 ratio to 13.8% of 1.5:1.2 ratio even if the COS value increased from 1.3±0.3% to 3.8±0.6%. To weaken the inhibition effect on m-BTP-PhC6 crystallization, a highly crystalline polymer donor (D18) was incorporated into PTQ10:m-BTP-PhC6 host system when PTQ10:m-BTP-PhC6 ratio was maintained as 1:1.2, and thus to simultaneously enhance the mechanical and photovoltaic performance. Impressively, the efficiency of ternary OSC with PTQ10:D18: m-BTP-PhC6 ratio as 1:0.5:1.2 (totally 1.5:1.2) remarkably increased from the corresponding binary films of 13.8% to 17.3%, together with the COS enhanced from 3.8±0.6% to 8.4±0.4% (highest 8.8%). The improvement in PCE was mainly attributed to the stronger crystallinity of m-BTP-PhC6 in ternary films and thus enhanced electron mobility compared with its binary counterpart. Detailed analysis revealed that D18 exhibited poor interaction with m-BTP-PhC6, which can liberate m-BTP-PhC6 molecules from PTQ10 domain. More importantly, concentrated m-BTP-PhC6 region in ternary blend films offers less D/A interface where cracks are easily to form and propagate, resulting much enhanced deformability than its binary counterpart with same D/A ratio. It should be noticed that the efficiency of 17.3% is the highest value reported in mechanically robust OSCs (with COS over 5%). Our work provides a useful guideline in diluting the small molecule content to design deformable OSCs with high efficiency from the view of interaction modulation.

RESULTS AND DISCUSSION

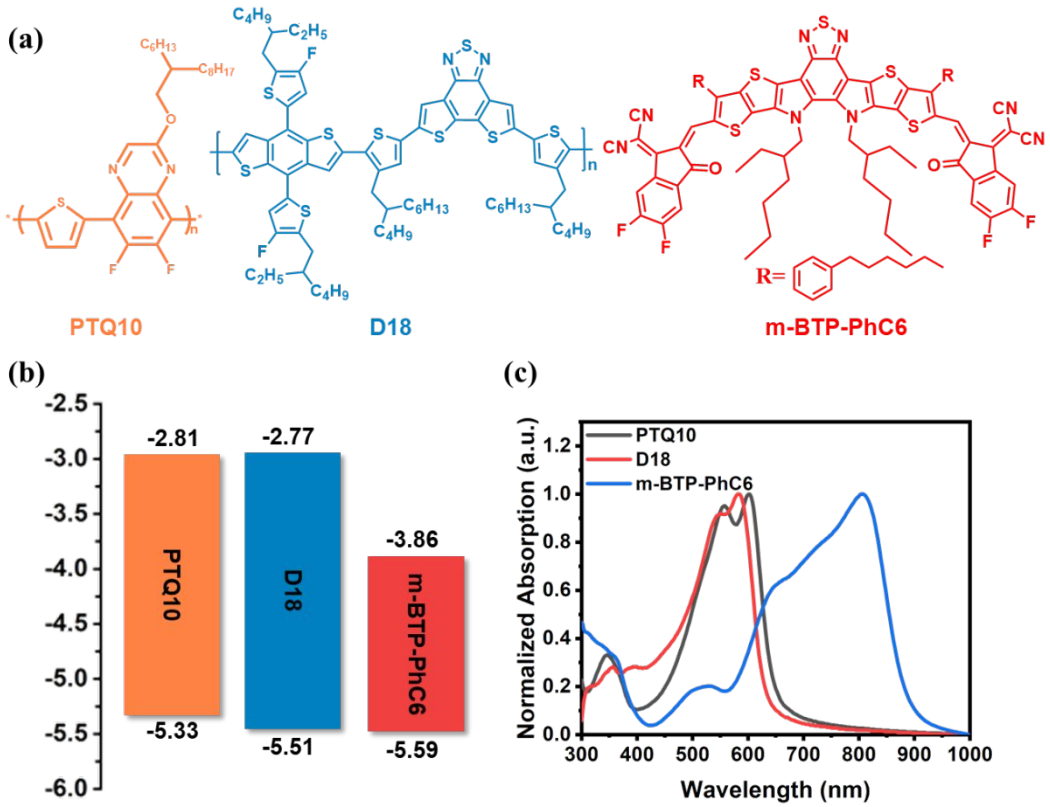

Fig. 1 (a) Chemical structures of PTQ10, D18 and m-BTP-PhC6. (b) The energy level diagram of PTQ10, D18 and m-BTP-PhC6. (c) UV-vis absorption of neat PTQ10, D18 and m-BTP-PhC6 films.

The molecular structures of PTQ10, D18 and m-BTP-PhC6 are shown in Fig. 1a and corresponding energy levels are concluded in Fig. 1b. Fig. 1c presents the absorption spectra of neat PTQ10, D18 and m-BTP-PhC6 films. PTQ10 and m-BTP-PhC6 exhibit strong absorption in 500-650 nm (absorption peak at 602 nm) and 600-900 nm (absorption peak at 804 nm), respectively. The third component D18 displays main absorption in the range of 400-600 nm with the absorption peak located at 582 nm. The absorption spectrum of PTQ10:D18 blend films with different D18 content is recorded in Fig. S1. The stronger absorption in the range of 500-550 nm can be observed in blend films, together with slight blue shift of PTQ10 absorption peak because of the addition of D18.

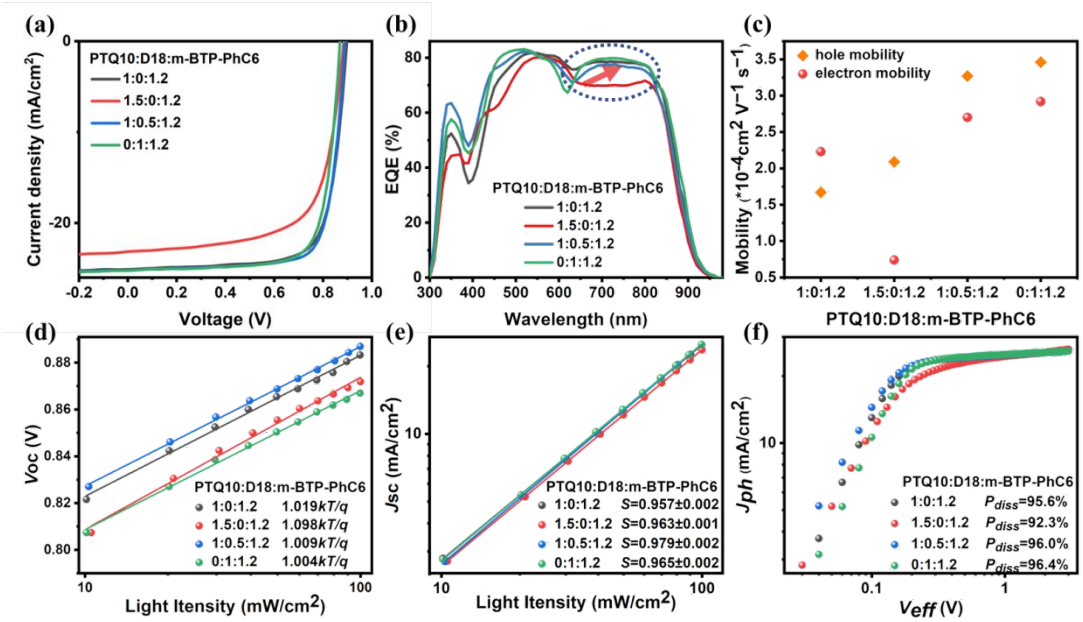

Fig. 2 (a) *J-V* curves of PTQ10:D18:m-BTP-PhC6 OSCs with ratio of 1:0:1.2, 1.5:0:1.2, 1:0.5:1.2 and 0:1:1.2 under AM 1.5G, 100 mA/cm^2. (b) EQE spectra, (c) Calculated mobility, light intensity dependence of (d) V_{oc}, (e) J_{sc} and (f)J_{ph} versus V_{eff} plots of PTQ10:D18: m-BTP-PhC6 OSCs with ratio of 1:0:1.2, 1.5:0:1.2, 1:0.5:1.2 and 0:1:1.2.

We firstly compared the effect of increased D/A ratio on the photovoltaic performance in binary and ternary systems, using conventional devices with the architecture of ITO/PEDOT:PSS/active layer/PDINO/Al. In this work, the D/A ratio in binary PTQ10:m-BTP-PhC6 system was changed from 1:1.2 to 1.2:1.2, 1.5:1.2 and 1.7:1.2. Correspondingly, ternary PTQ10:D18:m-BTP-PhC6 blends with total D/A ratio of 1.2:1.2 (1:0.2:1.2), 1.5:1.2 (1:0.5:1.2) and 1.7:1.2 (1:0.7:1.2) were fabricated by increasing D18 content when PTQ10:m-BTP-PhC6 relative ratio was maintained as 1:1.2. The *J-V* curves of these devices are exhibited in Fig. 2a and S2 and the relative detailed photovoltaic parameters are displayed in Table 1 and S1. Binary PTQ10: m-BTP-PhC6 and D18:m-BTP-PhC6 exhibit PCE of 16.7±0.1% and 16.6±0.1%, respectively. This PCE for PTQ10:m-BTP-PhC6 is comparable with the value (16.5±0.2%) reported by Cui and coworkers with the same active layer[34]. Meanwhile, this is the first time to report for the mixture of D18 with m-BTP-PhC6 as

the active layer to fabricate OSC. For binary PTQ10:m-BTP-PhC6 system, the best PCE decreased from 16.9% to 16.3%, 13.8% and 11.5% when the D/A ratio gradually increased from the optimized D/A ratio 1:1.2 to 1.7:1.2. In contrast, the corresponding ternary OSCs with total D/A ratio of 1.2:1.2, 1.5:1.2 and 1.7:1.2 exhibited much higher efficiency of 17.6%, 17.3% and 16.7% due to the remarkable enhancement in J_{sc} and fill factor (FF). The best photovoltaic performance for ternary PTQ10:D18:m-BTP-PhC6 system is achieved under D/A ratio of 1:0.2:1.2 with highest PCE of 17.6%, which is lower than the PCE of PTQ10:m-BTP-PhC6:PC71BM because of the different post treatments we used. The obvious promotion of EQE in the range from 650 to 810 nm (the absorption range of m-BTP-PhC6) overserved in the ternary system corresponds well with their much higher photocurrent compared with binary system under same total D/A ratio (Fig. 2b and S3). To better understand the enhancement of J_{sc} under large D/A ratio in ternary systems when compared with the BHJ counterparts, we measured the absorption coefficient of D18 and PTQ10 films (Figure S4). The absorption coefficients of D18 and PTQ10 are 9.26×10^4 cm^{-1} and 8.67×10^4 cm^{-1}, respectively. Higher absorption coefficient of D18 enables ternary films with enhanced light harvesting ability under large D/A ratio than the BHJ counterparts, corresponding well with the higher EQE response in the range from 450 to 550 nm for ternary blends.

Table 1 Summary of photovoltaic parameters of PTQ10:D18:m-BTP-PhC6 OSCs with ratio of 1:0:1.2, 1.5:0:1.2, 1:0.5:1.2 and 0:1:1.2 under AM 1.5G, 100 mA/cm^2.

PTQ10:D18:m-BTP-PhC6	V_{oc} (V)	J_{sc} (mA/cm^2)	FF (%)	Efficiency (%)
1:0:1.2	0.892±0.004	25.1±0.3	74.7±0.6	16.7±0.1
	0.899	25.1	74.9	16.9
1.5:0:1.2	0.883±0.004	23.4±0.4	66.2±0.9	13.7±0.1
	0.885	23.1	67.4	13.8
1:0.5:1.2	0.892±0.004	25.3±0.3	75.5±1.3	17.1±0.1

	0.890	25.2	77.2	17.3
0:1:1.2	0.869±0.004	25.2±0.2	75.7±0.7	16.6±0.1
	0.870	25.2	76.1	16.7

To understand the underlying mechanism of the better D/A ratio tolerance on FF in ternary system, device physics processes including charge transport and collection were analyzed. Mobility measured through space-charge-limited current (SCLC) is drawn in Fig. 2c and S4. In binary PTQ10:m-BTP-PhC6, the electron mobility of blends decreases with the increased D/A ratio, together with enhanced hole mobility (μ_h): electron mobility (μ_e) ratio from 0.75 of 1:1.2 to 4.08 of 1.7:1.2. This unbalanced μ_h:μ_e results in severe charge recombination and thus lower FF and J_{sc}. However, only small variation of electron mobility can be observed in ternary films as the D/A ratio increases. Consequently, ternary blends show stable and balanced μ_h:μ_e ranging from 1.12 to 1.21 along with increased D/A ratio, corresponding well to their high FF. We then measured the dependence of V_{oc} on light intensity (P) to study the trap-assisted recombination (Fig. 2d and S5a).[35] The slope of V_{oc} against P_{light} for binary PTQ10:m-BTP-PhC6 with different D/A ratio significantly promoted from 1.019 kT/q of 1:1.2 to 1.215 kT/q of 1.7:1.2, suggesting that trap-assisted recombination is more significant in large D/A ratio devices. As for ternary blend films, the slope is close to 1 kT/q against different D/A ratios, illustrating that only weak trap-assisted recombination occurs in these devices. The J_{SC} versus light intensity (P) which follows a power-law formula of $J_{sc} \propto P_{light}^{S}$ were recorded to analyze the bimolecular recombination (Fig. 2e and S5b).[36-38] The calculated exponent S for four binary PTQ10:m-BTP-PhC6 films slightly drops from 0.957±0.002 of 1:1.2 to 0.943±0.002 of 1.7:1.2, demonstrating that bimolecular recombination becomes more severe with increment in D/A ratio. The higher exponent S for three ternary blends in all three D/A ratio are in well agreement with their superior PCE.

To better explain the change of photocurrent in binary and ternary films with various D/A ratio, we compared the exciton dissociation and charge collection properties

through measuring photocurrent density (J_{ph}) versus effective voltage (V_{eff}) (Fig. 2f and S5c). J_{ph} represents the difference between J_L and J_D, where J_L and J_D are the current densities values under standard illumination condition and in the dark condition, respectively. V_{eff} is defined as the variation between V_0 and V_{bias}, in which V_0 is the voltage value when J_{ph} is zero and V_{bias} is the external voltage bias value.[39] Exciton dissociation probability (P_{diss}) of four binary PTQ10:m-BTP-PhC6 devices is 95.6%, 93.3%, 92.3% and 91.9%, while these three ternary blends possess similar P_{diss} around 96% when the D/A ratio increased. Poor P_{diss} obtained in binary devices with high D/A ratio correlates well with the much deteriorated photocurrent. The lower photoluminescence (PL) quenching efficiency in binary films than their ternary counterparts revealed by PL spectra (Fig. S6) also confirmed the deteriorated exciton dissociation in binary system when D/A ratio increased. Therefore, the higher exciton dissociation probability as well as the more efficient quenching efficiency all prove that the incorporation of D18 helps the ternary blends to maintain stable photocurrent under larger D/A ratio.

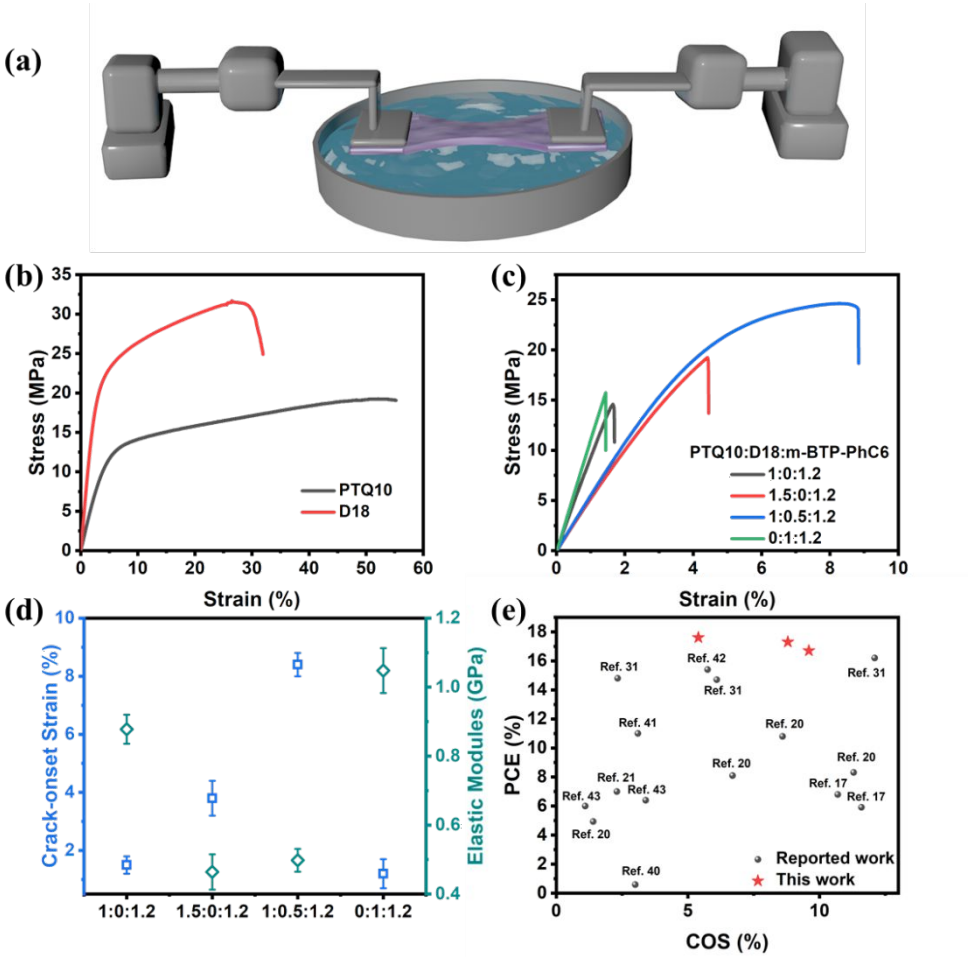

Fig. 3 (a) Diagram of film on water (FOW) tensile test equipment. (b) Strain-stress curves of (b) neat PTQ10 and D18, (c) PTQ10:D18:m-BTP-PhC6 blend films with ratio of 1:0:1.2, 1.5:0:1.2, 1:0.5:1.2 and 0:1:1.2. (d) Extracted crack-onset strain and elastic modules versus different PTQ10:D18:m-BTP-PhC6 ratios. (e) Distribution of PCEs of OSCs versus COS values (measured by FOW tensile test) in the reported polymer/small molecule systems and this study[17, 20, 21, 31, 40-43].

After checking the dependence of photovoltaic performance on increased D/A ratio in binary and ternary systems, we measured the stress-strain curves of these films using film on water (FOW) tensile measurement[44] to illuminate the effect of changing D/A ratio on mechanical properties**.** Diagram of FOW tensile test, where the measured films are floated onto water and the load and displacement recording elements are adhered to these films, is drawn in Fig. 3a. We firstly compared the mechanical properties of these three materials used in this work. Unfortunately, the stress-strain

curves of pure m-BTP-PhC6 could not be successfully recorded through FOW test as the result of its brittleness, making it crack during floating the film onto water.[45] PTQ10 and D18 used in this work have number-average molecular weights within a similar range to minimize the impact of molecular weight on material properties (Fig. S7)[46-48]. Because of the high molecular weight, both neat PTQ10 and D18 films can induce sufficient intermolecular entanglements, and thus are highly mechanically stretchable with the COS of 50.1±5.2% and 28.3±2.9%, respectively (Fig. 3b). Nonetheless, blending m-BTP-PhC6 with highly ductile PTQ10 or D18 still returns a limited mechanical deformability (Fig. 3c and d) (the COS of 1.3±0.3% and elastic modules (E_f) of 0.878±0.042 GPa for PTQ10:m-BTP-PhC6 and the COS of 1.2±0.2% and E_f of 1.048±0.065 GPa for D18:m-BTP-PhC6). This significant embrittlement after mixing with m-BTP-PhC6 is caused by introduction of brittle interfacial area, where cracks tend to form and propagate due to remarkable difference of elastic modules between ductile polymer and brittle small molecule.[49] Increasing the D/A ratio in binary PTQ10: m-BTP-PhC6 softens the blend films with higher COS and lower E_f value (Fig. 3d and S8) as the result of less D/A interface caused by diluted m-BTP-PhC6 content. Unexpectedly, the mechanical performance of ternary systems with same D/A ratio all outperformed their binary counterparts (Fig. 3d and S8). Specifically, ternary systems with D/A ratio of 1.2:1.2, 1.5:1.2 and 1.7:1.2 has a higher COS of 5.1±0.3%, 8.4±0.4% and 8.9±0.7% than its binary counterpart of 2.9%, 4.4% and 6.3%. We speculate this may be related to the morphological difference between binary and ternary systems, which we will discuss specifically in the following section. As shown in Fig. 3e, the highest PCE value of OSCs in the reported literatures with COS value of active layers measured above 5% is 16.7% till now, which is reported by Kim and coworkers in Ref. 31. In contrast, the highest efficiency of PTQ10:D18:m-BTP-PhC6 system with D/A ratio of 1:0.5:1.2 is 17.3%, together with a COS of 8.8%. It should be noticed that we have achieved the highest efficiency in OSCs with COS over 5%, illustrating that diluting the small molecule content is an effective method to fabricate high-efficiency while mechanically deformable OSCs.

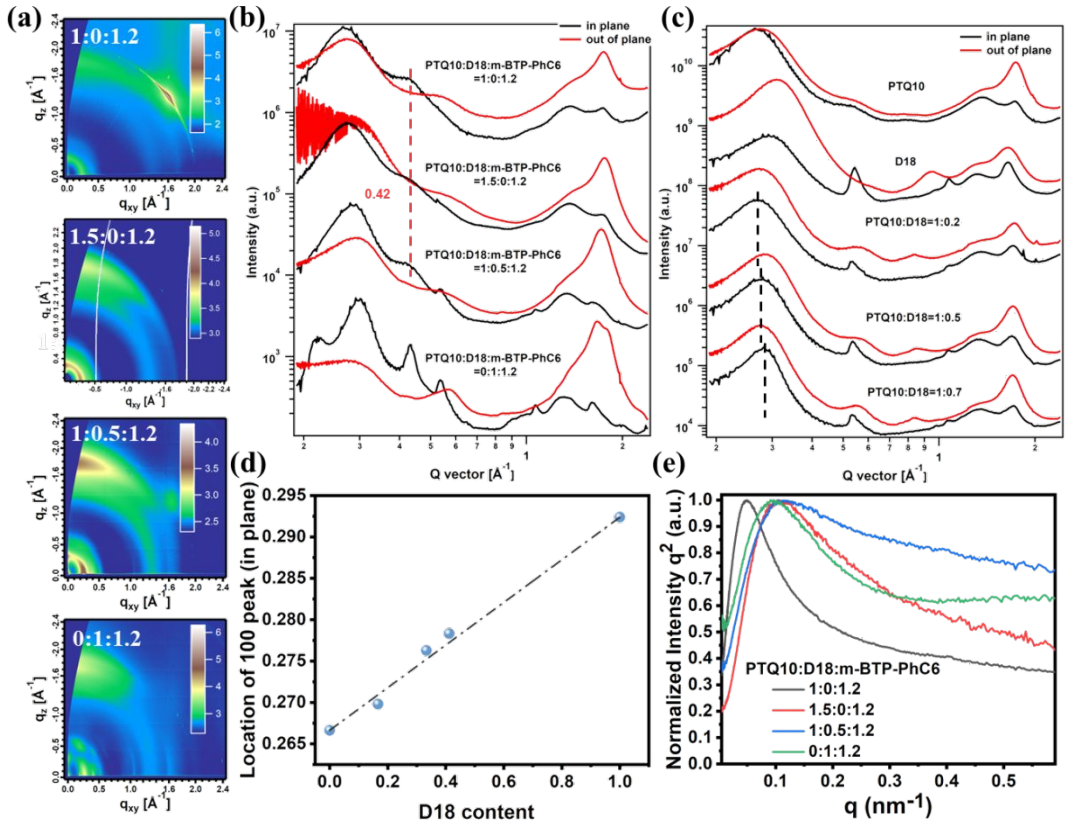

Fig. 4 (a) The 2D GIWAXS profiles and (b) in-plane and out-of-plane GIWAXS profiles of PTQ10:D18:m-BTP-PhC6 with ratio of 1:0:1.2, 1.5:0:1.2, 1:0.5:1.2 and 0:1:1.2. (c) In-plane and out-of-plane GIWAXS profiles of PTQ10:D18 blends with different D18 content. (d) Calculated 100 peak location along in plane direction of binary PTQ10:D18 blends as the function of D18 content. (e) Normalized RSoXS profiles of PTQ10:D18: m-BTP-PhC6 with ratio of 1:0:1.2, 1.5:0:1.2, 1:0.5:1.2 and 0:1:1.2.

Figuring out the role of D18 on morphology is of crucial importance to understand the divergent dependence of binary and ternary systems on D/A ratio. Grazing-incidence wide-angle X-ray scattering (GIWAXS) was carried out to probe the molecular packing and crystallinity, which can be expressed by calculating d-spacing and coherence length (CL), of the photoactive films.[50] As shown in Fig. S9 and 10, neat m-BTP-PhC6 and D18 show characteristic peaks at 0.42 (d-spacing of 1.49 nm) and 0.54 $Å^{-1}$ (d-spacing of 1.16 nm) along the in plane direction, respectively. The

characteristic crystalline peak of m-BTP-PhC6 can be clearly differentiated in PTQ10:m-BTP-PhC6 with D/A ratio of 1:1.2 (CL of 7.20 nm and d-spacing of 1.48 nm in Table 2). However, this peak becomes much weaker when the D/A ratio increased and almost disappears in 1.7:1.2 binary film (Fig. S10), indicating the strong inhibition of m-BTP-PhC6 crystallization from the interaction of PTQ10. The largely decreased crystallinity of m-BTP-PhC6 in binary PTQ10: m-BTP-PhC6 films when D/A ratio increased results in the significant deterioration of electron mobility and thus remarkable drop in photovoltaic performance. Moreover, this inhibition effect can also be confirmed by the significant decrease in absorption of m-BTP-PhC6 as recorded in Fig. S11. In contrast, the crystallinity of m-BTP-PhC6 is not severely abrupted after incorporating 50% D18, which exhibits comparable CL (7.13 nm) and d-spacing (1.49 nm) values compared to its binary counterpart (Table 2). This unchanged crystallinity of m-BTP-PhC6 indicates the poor interaction between D18 and m-BTP-PhC6. Moreover, we calculated the (100) peak location along in plane direction of PTQ10:D18 films with various D18 content to portray the interaction between PTQ10 and D18 (Fig. 4d). The (100) peak of pure PTQ10 and D18 along in plane direction locates at 0.267 and 0.292 $Å^{-1}$, respectively. The (100) peak location of binary PTQ10:D18 blends locate between 0.267 and 0.292 $Å^{-1}$ following a linear function of D18 content (Fig. 4d), which indicates the weak interaction between PTQ10 and D18. Therefore, the well maintained crystallinity of m-BTP-PhC6 in ternary PTQ10:D18:m-BTP-PhC6 as the D/A ratio increased enabled by the poor interaction between D18 and m-BTP-PhC6 ensures superior electron transportation and thus high device efficiency.

Table 2 Crystallinity parameters of different photovoltaic films.

PTQ10:D18:m-BTP-PhC6	Characteristic peak of m-BTP-PhC6 (In plane)	
	d-spacing(nm)	CL(nm)
1:0:1.2	1.48	7.20
1:0.5:1.2	1.49	7.13

0:1:1.2	1.45	19.6

Miscibility is another effective method to evaluate the interaction between different materials.[51] Herein, contact angle measurement was employed to analyze the miscibility between D18, PTQ10 and m-BTP-PhC6. The corresponding images of water and glycerol droplets on the neat D18, PTQ10 and m-BTP-PhC6 films are shown in Fig. S12 and the calculated surface free energy (γ_s) are 34.09, 26.97 and 45.42 mN/m, respectively (Table S2). Correspondingly, the solubility parameters (δ), which are proportional to the square root of the surface energy, are calculated to be 21.42, 19.05 and 45.42 $MPa^{1/2}$, respectively. According to the Flory–Huggins model[52, 53], the calculated interaction parameters between D18 and PTQ10 is 0.522 and that between D18 and m-BTP-PhC6 is 0.694. The high and similar interaction parameters between D18 and the other two materials indicate that D18 shows weak interaction with PTQ10 or m-BTP-PhC6. The results from contact angle measurements can well support the observation obtained in GIWAXS measurement.

Table 3 The Phase Separation Parameters of PTQ10:D18:m-BTP-PhC6 blend films with ratio of 1:0:1.2, 1.5:0:1.2, 1:0.5:1.2 and 0:1:1.2.

PTQ10:D18:m-BTP-PhC6	Location (nm^{-1})	Domain size (nm)
1:0:1.2	0.0610	51.5
1.5:0:1.2	0.129	24.4
1:0.5:1.2	0.137	22.9
0:1:1.2	0.105	29.8

Resonant soft X-ray scattering (RSoXS), transmission electron microscopy (TEM) and atomic force microscope were performed to detect the phase separation in these films. We choose X-ray energy of 284.8 eV to ensure the highest scattering contrast of these organic materials.[54] Fig. 4e and S13 record the normalized RSoXS profiles of PTQ10:D18:m-BTP-PhC6 with various D/A ratio and the calculated domain size is listed in Table 3 and S3. In binary PTQ10:m-BTP-PhC6 films, domain size varies

from 54.5 nm to 40.4, 24.4 and 21.6 nm when D/A ratio increases from 1:1.2 to 1.2:1.2, 1.5:1.2 and 1.7:1.2, respectively. The stronger inhibition of PTQ10 to m-BTP-PhC6 under larger D/A ratio makes m-BTP-PhC6 difficult to form m-BTP-PhC6-rich region, resulting in smaller domain size in binary PTQ10:m-BTP-PhC6 system.[55] Ternary blends with 1.2:1.2, 1.5:1.2 and 1.7:1.2 exhibit similar domain size with their binary counterparts, which is 35.6, 22.9 and 20.9 nm, respectively. TEM images shown in Fig. S14 indicates that all binary PTQ10:m-BTP-PhC6 films exhibit homogeneous phase distribution and become more homogeneous as the D/A ratio increased. In contrast, the ternary systems display much more obvious phase separation in comparison with their binary counterparts due to the inferior miscibility between D18 and host two materials. Similar domain size combined with more obvious phase separation enable ternary films with reduced interfacial area than the binary counterparts under same D/A ratio, leading to the higher stretchability of ternary blends than the corresponding binary ones. Because of the strong tendency of D18 to crystallize and the poor interaction between D18 and m-BTP-PhC6, obvious fiber-like structure induced by D18 can be observed in binary D18:m-BTP-PhC6 film, which is favorable for charge transport.[56, 57] Ternary films retain the fibril structure of D18 and this structure becomes more apparent with increased addition of D18, which is beneficial for the charge transport under high D/A ratio. Moreover, this clear fibril morphology of D18 also helps to prove the poor miscibility between D18 and PTQ10: m-BTP-PhC6 matrix. Surface morphology evolution of these blend films are determined by AFM test. As shown in Fig. S15, the surface roughness of binary PTQ10:m-BTP-PhC6 systems decreases with higher D/A ratio from 1.36 nm of 1:1.2 to 0.697 nm of 1.7:1.2, correlating well with the smaller phase separation in blends with larger D/A ratio observed in RSoXS.[49] This D/A ratio dependent relationship also occurs in ternary PTQ10:D18:m-BTP-PhC6 systems.

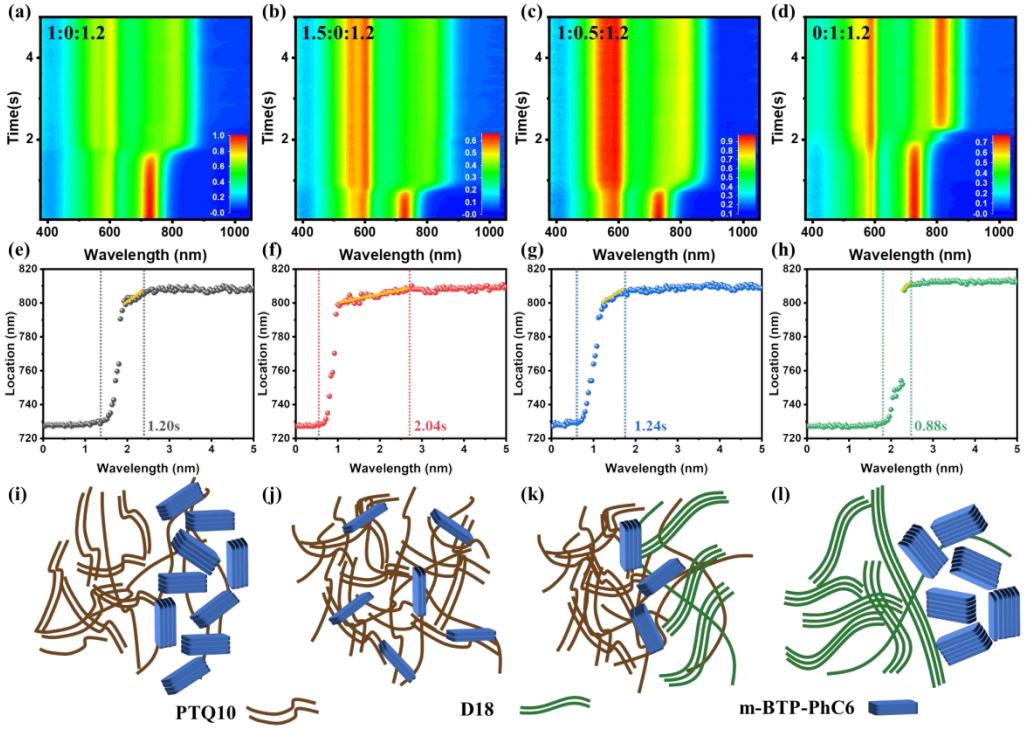

Fig. 5 (a)-(d) Time-dependent contour maps of UV-vis absorption spectra, (e)-(h) time evolution of peak location of m-BTP-PhC6 and (i)-(l) diagram of morphology of PTQ10:D18:m-BTP-PhC6 with ratio of 1:0:1.2, 1.5:0:1.2, 1:0.5:1.2 and 0:1:1.2

In order to illuminate the role of D18 on enhancing the D/A ratio tolerance in ternary blends, we performed in-situ studies on morphology evolutions during film drying. Fig. 5(a)-(d) and S16 show the time evolution of UV-vis absorption contour maps of PTQ10:D18:m-BTP-PhC6 with different relative ratio. The corresponding raw in-situ UV-vis absorption spectra are shown in Fig. S17. The UV-vis absorption spectra are transformed from the transmission spectra based on the equation that $A\lambda=-\log_{10}(T)$, where A_λ is the absorbance at a certain wavelength (λ) and T is the measured transmittance after background correction using blank glass.[58] The evolution of peak location in UV-vis absorption reveals the change of aggregation of donor or acceptor. In all the binary PTQ10:m-BTP-PhC6 films, both the peak location of PTQ10 and m-BTP-PhC6 are red-shifted when solvent evaporated, suggesting that the simultaneous aggregation of PTQ10 and m-BTP-PhC6 occurred. However, no obvious red-shift of D18 can be observed in D18:m-BTP-PhC6 during the solvent

evaporation. Incorporating D18 into PTQ10:m-BTP-PhC6 stabilizes the aggregation of PTQ10 as revealed by the nearly identical peak location of PTQ10 across the whole film-drying process in all three ternary films.

The time evolution of m-BTP-PhC6 peak location in these films is extracted from in-situ UV-vis absorption spectrum to directly understand the influence of PTQ10 and D18 on the aggregation behavior of m-BTP-PhC6 and the relative results are exhibited in Fig. 5(e)-(h) and S18. The peak location evolution of these films can be divided into three stages. For the first stage, the peak location of m-BTP-PhC6 does not vary with solvent evaporation. In the second stage, the absorption peak location of m-BTP-PhC6 shifts to NIR region as solvent evaporates since solution concentration crosses the solubility limit and reaches critical supersaturation. Finally, the peak location of m-BTP-PhC6 reaches constant at the third stage. For binary PTQ10:m-BTP-PhC6 systems, the duration of the second stage prolongs as the D/A ratio increases, significantly varying from 1.2s for 1:1.2 to 2.04s for 1.5:1.2. The larger number of PTQ10 molecules in binary PTQ10:m-BTP-PhC6 systems confines the movement of m-BTP-PhC6. Therefore, m-BTP-PhC6 molecules need to take longer time to firstly come out from the donor region and then to form aggregates. As the result of stronger confinement of PTQ10 to m-BTP-PhC6 under higher D/A ratio, m-BTP-PhC6 cannot form sufficient self-aggregation region to maintain the continuous interpenetrating network, which is harmful for electron mobility and photovoltaic performance. Because of the poor interaction between D18 and m-BTP-PhC6, D18:m-BTP-PhC6 binary film exhibits shortest time of 0.88s of the second stage. Adding 50% D18 into PTQ10:m-BTP-PhC6 to construct ternary blend with D/A ratio of 1.5:1.2 shortens the duration time of second stage to 1.24s, which is comparable with that of binary PTQ10:m-BTP-PhC6 with D/A ratio of 1:1.2. The easy aggregation of m-BTP-PhC6 in ternary blends ensures the efficient crystallization of m-BTP-PhC6 and the formation of interconnected interpenetrating network under large D/A ratio, resulting in the much higher PCE than binary PTQ10: m-BTP-PhC6.

With the help of multiple morphology characterization measurements, the

morphology of PTQ10:D18:m-BTP-PhC6 with ratio of 1:0:1.2, 1.5:0:1.2, 1:0.5:1.2 and 0:1:1.2 can be depicted as the pictures shown in Fig. 5(i)-(l). For PTQ10:m-BTP-PhC6 with D/A ratio of 1:1.2, m-BTP-PhC6 can easily form large aggregated region of m-BTP-PhC6 with relative higher crystallinity due to the low content of PTQ10, resulting in large domain size. With the D/A ratio increases to 1.5:1.2, the uniformly dispersed m-BTP-PhC6 molecules in PTQ10 matrix are difficult to aggregate and crystallize from the strong inhibition of PTQ10, leading to homogeneously distributed domain with lower crystallinity and small domain size. This insufficient aggregation of m-BTP-PhC6 breaks the continuity of the interpenetrating network and thus decreases the photovoltaic performance. Nevertheless, the smaller volume of m-BTP-PhC6 benefits the mechanical ductility of binary PTQ10: m-BTP-PhC6 with D/A ratio of 1.5:1.2. For ternary blends with 50% addition of D18, the poor miscibility between D18 and m-BTP-PhC6 promise the effective aggregation and crystallinity of m-BTP-PhC6. This large number of aggregated m-BTP-PhC6 molecules not only contribute to the efficient charge transport but also enable ternary blends with less interface and thus higher stretchability than its binary counterpart.[49] The highest crystallinity of m-BTP-PhC6 with largest aggregated region achieved in binary D18:m-BTP-PhC6 blend film, together with the strong crystallinity of D18 result in its poorest mechanical performance.

Conclusions

In summary, we have developed a series of high-efficiency while mechanical robust OSCs by incorporating relative immiscible polymer donor (D18) into PTQ10: m-BTP-PhC6 system to dilute the content of brittle small molecule (m-BTP-PhC6). It was found that directly increasing the content of PTQ10 in binary PTQ10: m-BTP-PhC6 blends indeed promoted the deformability of photovoltaic films as the result of reduction of debonding sites along brittle interface. However, the photon-to -electron conversion efficiency also significantly decreased due to the largely restricted crystallinity of m-BTP-PhC6 by PTQ10. Replacing PTQ10 with D18 not only can effectively boost the photovoltaic performance but also benefits the mechanical stretchability, resulting in the balanced high efficiency of 17.3% and superior deformability of 8.8%. Augmented PCE under large D/A ratio in ternary blends stems from the largely improved crystallinity of m-BTP-PhC6 and thus well maintained percolation pathways, as the result of poor interaction between D18 and m-BTP-PhC6. More importantly, larger aggregated region of m-BTP-PhC6 enables the ternary systems with less interfacial area as compared to their binary counterparts. Our work clearly demonstrates that highly efficient polymer:small molecule OSCs with superior mechanical reliability can be achieved through diluting the content of small molecules with proper control over the molecular interaction.

Author contributions

Zhu Qinglian: Conceptualization, Methodology, Validation, Investigation, Writing – Original Draft. Xue Jingwei: Investigation. Zhao Heng: Investigation. Lin Baojun: Investigation. Bi Zhaozhao: Writing - Review & Editing. Seibt Susanne: Investigation. Zhou Ke: Writing - Review & Editing. Ma Wei: Conceptualization, Methodology, Resources, Writing - Review & Editing, Supervision, Project administration, Funding acquisition.

Conflict of Interest

The authors declare no conflict of interest.

ACKNOWLEDGMENTS

Thanks for the support from NSFC (21704082, 21875182). The GIWAXS data of this research was undertaken on the SAXS/WAXS beamline at the Australian Synchrotron, part of ANSTO. The authors thank Dr. Nigel Kirby for assistance with data acquisition. RSoXS data was acquired at beamline 11.0.1.2 at the Advanced Light Source, which is supported by the Director, Office of Science, Office of Basic Energy Sciences, of the U.S. Department of Energy under Contract No. DE-AC02-05CH11231.

REFERENCE

1. F. C. Krebs, T. D. Nielsen, J. Fyenbo, M. Wadstrøm and M. S. Pedersen, *Energy Environ. Sci.*, 2010, **3**, 512-525.
2. C. Lee, S. Lee, G.-U. Kim, W. Lee and B. J. Kim, *Chem. Rev.*, 2019, **119**, 8028-8086.
3. G.-J. N. Wang, A. Gasperini and Z. Bao, *Adv. Electron. Mater.*, 2018, **4**, 1700429.
4. C. Cui and Y. Li, *Energy Environ. Sci.*, 2019, **12**, 3225-3246.
5. C. Zhu, L. Meng, J. Zhang, S. Qin, W. Lai, B. Qiu, J. Yuan, Y. Wan, W. Huang and Y. Li, *Adv. Mater.*, 2021, **33**, 2100474.
6. Q. Liu, Y. Jiang, K. Jin, J. Qin, J. Xu, W. Li, J. Xiong, J. Liu, Z. Xiao, K. Sun, S. Yang, X. Zhang and L. Ding, *Sci. Bull.*, 2020, **65**, 272-275.
7. C. Yang, Q. An, H. R. Bai, H. F. Zhi, H. S. Ryu, A. Mahmood, X. Zhao, S. Zhang, H. Y. Woo and J. L. Wang, *Angew. Chem. Int. Ed. Engl.*, 2021, **133**, 19390-19401.
8. G. Chai, Y. Chang, J. Zhang, X. Xu, L. Yu, X. Zou, X. Li, Y. Chen, S. Luo, B. Liu, F. Bai, Z. Luo, H. Yu, J. Liang, T. Liu, K. S. Wong, H. Zhou, Q. Peng and H. Yan, *Energy Environ. Sci.*, 2021, **14**, 3469-3479.
9. P. Bi, S. Zhang, Z. Chen, Y. Xu, Y. Cui, T. Zhang, J. Ren, J. Qin, L. Hong, X. Hao and J. Hou, *Joule*, 2021, **5**, 2408-2419.
10. Y. Cui, Y. Xu, H. Yao, P. Bi, L. Hong, J. Zhang, Y. Zu, T. Zhang, J. Qin, J. Ren, Z. Chen, C. He, X. Hao, Z. Wei and J. Hou, *Adv. Mater.*, 2021, **33**, 2102420.
11. M. Zhang, L. Zhu, G. Zhou, T. Hao, C. Qiu, Z. Zhao, Q. Hu, B. W. Larson, H. Zhu, Z. Ma, Z. Tang, W. Feng, Y. Zhang, T. P. Russell and F. Liu, *Nat. Commun.*, 2021, **12**, 309.
12. K. Jin, Z. Xiao and L. Ding, *J. Semicond.*, 2021, **42**, 060502.
13. S. Savagatrup, A. D. Printz, H. Wu, K. M. Rajan, E. J. Sawyer, A. V. Zaretski, C. J. Bettinger and D. J. Lipomi, *Synth. Met.*, 2015, **203**, 208-214.
14. O. Awartani, B. I. Lemanski, H. W. Ro, L. J. Richter, D. M. DeLongchamp and B. T. O'Connor, *Adv. Energy Mater.*, 2013, **3**, 399-406.
15. W. Huang, Z. Jiang, K. Fukuda, X. Jiao, C. R. McNeill, T. Yokota and T. Someya, *Joule*, 2020, **4**, 128-141.
16. Z. Peng, K. Xian, Y. Cui, Q. Qi, J. Liu, Y. Xu, Y. Chai, C. Yang, J. Hou, Y. Geng and L. Ye, *Adv. Mater.*, 2021, **33**, 2106732.
17. W. Lee, J.-H. Kim, T. Kim, S. Kim, C. Lee, J.-S. Kim, H. Ahn, T.-S. Kim and B. J. Kim, *J. Mater. Chem. A*, 2018, **6**, 4494-4503.
18. H. You, A. Jones, B. S. Ma, G.-U. Kim, S. Lee, J.-W. Lee, H. Kang, T.-S. Kim, J. R. Reynolds and B. Kim, *J. Mater. Chem. A*, 2021, **9**, 2775-2783.
19. T. Kim, J.-H. Kim, T. E. Kang, C. Lee, H. Kang, M. Shin, C. Wang, B. Ma, U. Jeong, T.-S. Kim and B. J. Kim, *Nat. Commun.*, 2015, **6**, 8547.
20. Q. Fan, W. Su, S. Chen, W. Kim, X. Chen, B. Lee, T. Liu, U. A. Méndez-Romero, R. Ma, T. Yang, W. Zhuang, Y. Li, Y. Li, T.-S. Kim, L.

Hou, C. Yang, H. Yan, D. Yu and E. Wang, *Joule*, 2020, **4**, 658-672.
21. J. W. Lee, C. Sun, B. S. Ma, H. J. Kim, C. Wang, J. M. Ryu, C. Lim, T. S. Kim, Y. H. Kim, S. K. Kwon and B. J. Kim, *Adv. Energy Mater.*, 2020, **11**, 2003367.
22. J.-W. Lee, B. S. Ma, J. Choi, J. Lee, S. Lee, K. Liao, W. Lee, T.-S. Kim and B. J. Kim, *Chem. Mater.*, 2020, **32**, 582–594.
23. H. Fu, Y. Li, J. Yu, Z. Wu, Q. Fan, F. Lin, H. Y. Woo, F. Gao, Z. Zhu and A. K. Jen, *J. Am. Chem. Soc.*, 2021, **143**, 2665-2670.
24. W. Wang, Q. Wu, R. Sun, J. Guo, Y. Wu, M. Shi, W. Yang, H. Li and J. Min, *Joule*, 2020, **4**, 1070-1086.
25. Y. Wang, N. Wang, Q. Yang, J. Zhang, J. Liu and L. Wang, *J. Mater. Chem. A*, 2021, **9**, 21071-21077.
26. H. Sun, B. Liu, Y. Ma, J. W. Lee, J. Yang, J. Wang, Y. Li, B. Li, K. Feng, Y. Shi, B. Zhang, D. Han, H. Meng, L. Niu, B. J. Kim, Q. Zheng and X. Guo, *Adv. Mater.*, 2021, **33**, 2102635.
27. H. Yu, S. Luo, R. Sun, I. Angunawela, Z. Qi, Z. Peng, W. Zhou, H. Han, R. Wei, M. Pan, A. M. H. Cheung, D. Zhao, J. Zhang, H. Ade, J. Min and H. Yan, *Adv. Funct. Mater.*, 2021, **31**, 2100791.
28. H. Yu, Z. Qi, J. Yu, Y. Xiao, R. Sun, Z. Luo, A. M. H. Cheung, J. Zhang, H. Sun, W. Zhou, S. Chen, X. Guo, X. Lu, F. Gao, J. Min and H. Yan, *Adv. Energy Mater.*, 2020, **11**, 2003171.
29. F. P. V. Koch, J. Rivnay, S. Foster, C. Müller, J. M. Downing, E. Buchaca-Domingo, P. Westacott, L. Yu, M. Yuan, M. Baklar, Z. Fei, C. Luscombe, M. A. McLachlan, M. Heeney, G. Rumbles, C. Silva, A. Salleo, J. Nelson, P. Smith and N. Stingelin, *Prog. Polym. Sci.*, 2013, **38**, 1978-1989.
30. E. Dauzon, X. Sallenave, C. Plesse, F. Goubard, A. Amassian and T. D. Anthopoulos, *Adv. Mater.*, 2021, **33**, 2101469.
31. J.-W. Lee, D. Jeong, D. J. Kim, T. N.-L. Phan, J. S. Park, T.-S. Kim and B. J. Kim, *Energy Environ. Sci.*, 2021, **14**, 4067-4076.
32. J. W. Lee, B. S. Ma, H. J. Kim, T. S. Kim and B. J. Kim, *JACS Au*, 2021, **1**, 612-622.
33. Z. Peng, K. Jiang, Y. Qin, M. Li, N. Balar, B. T. O'Connor, H. Ade, L. Ye and Y. Geng, *Adv. Energy Mater.*, 2021, **11**, 2003506.
34. S. Bao, H. Yang, H. Fan, J. Zhang, Z. Wei, C. Cui and Y. Li, *Adv. Mater.*, 2021, **33**, 2105301.
35. W. L. Leong, S. R. Cowan and A. J. Heeger, *Adv. Energy Mater.*, 2011, **1**, 517-522.
36. Y. Qin, M. A. Uddin, Y. Chen, B. Jang, K. Zhao, Z. Zheng, R. Yu, T. J. Shin, H. Y. Woo and J. Hou, *Adv. Mater.*, 2016, **28**, 9416-9422.
37. S. R. Cowan, A. Roy and A. J. Heeger, *Phys. Rev. B*, 2010, **82**, 245207.
38. Y. Zang, C.-Z. Li, C.-C. Chueh, S. T. Williams, W. Jiang, Z.-H. Wang, J.-S. Yu and A. K.-Y. Jen, *Adv. Mater.*, 2014, **26**, 5708-5714.
39. P. W. M. Blom, V. D. Mihailetchi, L. J. A. Koster and D. E. Markov, *Adv. Mater.*, 2007, **19**, 1551-1566.

40. S. Savagatrup, A. S. Makaram, D. J. Burke and D. J. Lipomi, *Adv. Funct. Mater.*, 2014, **24**, 1169-1181.
41. Y. Wang, Q. Zhu, H. B. Naveed, H. Zhao, K. Zhou and W. Ma, *Adv. Energy Mater.*, 2020, **10**, 1903609.
42. J. Han, F. Bao, D. Huang, X. Wang, C. Yang, R. Yang, X. Jian, J. Wang, X. Bao and J. Chu, *Adv. Funct. Mater.*, 2020, **30**, 2003654.
43. J. Choi, W. Kim, S. Kim, T.-S. Kim and B. J. Kim, *Chem. Mater.*, 2019, **31**, 9057-9069.
44. J. H. Kim, A. Nizami, Y. Hwangbo, B. Jang, H. J. Lee, C. S. Woo, S. Hyun and T. S. Kim, *Nat. Commun.*, 2013, **4**, 2520.
45. S. Zhang, M. U. Ocheje, S. Luo, D. Ehlenberg, B. Appleby, D. Weller, D. Zhou, S. Rondeau-Gagne and X. Gu, *Macromol. Rapid Commun.*, 2018, **39**, 1800092.
46. D. K. Tran, A. Robitaille, I. J. Hai, X. Ding, D. Kuzuhara, T. Koganezawa, Y.-C. Chiu, M. Leclerc and S. A. Jenekhe, *J. Mater. Chem. A*, 2020, **8**, 21070-21083.
47. C. Bruner and R. Dauskardt, *Macromolecules*, 2014, **47**, 1117-1121.
48. Z. Li, W. Zhong, L. Ying, F. Liu, N. Li, F. Huang and Y. Cao, *Nano Energy*, 2019, **64**.
49. J.-H. Kim, J. Noh, H. Choi, J.-Y. Lee and T.-S. Kim, *Chem. Mater.*, 2017, **29**, 3954-3961.
50. A. Hexemer, W. Bras, J. Glossinger, E. Schaible, E. Gann, R. Kirian, A. MacDowell, M. Church, B. Rude and H. Padmore, *J. Phys. Conf. Ser.*, 2010, **247**, 012007.
51. S. Holliday, R. S. Ashraf, A. Wadsworth, D. Baran, S. A. Yousaf, C. B. Nielsen, C.-H. Tan, S. D. Dimitrov, Z. Shang, N. Gasparini, M. Alamoudi, F. Laquai, C. J. Brabec, A. Salleo, J. R. Durrant and I. McCulloch, *Nat. Commun.*, 2016, **7**, 11585.
52. S. Nilsson, A. Bernasik, A. Budkowski and E. Moons, *Macromolecules*, 2007, **40**, 8291-8301.
53. J. A. Emerson, D. T. W. Toolan, J. R. Howse, E. M. Furst and T. H. Epps, *Macromolecules*, 2013, **46**, 6533-6540.
54. E. Gann, A. T. Young, B. A. Collins, H. Yan, J. Nasiatka, H. A. Padmore, H. Ade, A. Hexemer and C. Wang, *Rev. Sci. Instrum.*, 2012, **83**, 045110.
55. J. Xin, X. Meng, X. Xu, Q. Zhu, H. B. Naveed and W. Ma, *Matter*, 2019, **1**, 1316-1330.
56. D. Li, C. Guo, X. Zhang, B. Du, C. Yu, P. Wang, S. Cheng, L. Wang, J. Cai, H. Wang, D. Liu, H. Yao, Y. Sun, J. Hou and T. Wang, *Sci. China Chem.*, 2021, DOI: 10.1007/s11426-021-1128-1.
57. H. Chen, T. Zhao, L. Li, P. Tan, H. Lai, Y. Zhu, X. Lai, L. Han, N. Zheng, L. Guo and F. He, *Adv. Mater.*, 2021, **33**, 2102778.
58. M. Abdelsamie, K. Zhao, M. R. Niazi, K. W. Chou and A. Amassian, *J. Mater. Chem. C*, 2014, **2**, 3373-3381.